First ion source at ISOL@MYRRHA with an improved thermal profile - Theoretical considerations

S Hurier[1,2], K Rijpstra[1], J P Ramos[1], L Popescu[1], T E Cocolios[2], R Mancheva[2,3], K Chrysalidis[3], S Rothe[3], M Au[3], and A Koliatos[3]

[1]Belgian Nuclear Research Centre, SCK CEN, Mol, Belgium,
[2]KU Leuven, Institute for Nuclear and Radiation Physics (IKS), Leuven, Belgium.
[3]CERN, Geneva, Switzerland

E-mail: sophie.hurier@sckcen.be

Abstract. ISOL@MYRRHA will be a new Radioactive Ion Beam (RIB) facility in Belgium based on the Isotope Separation On-Line (ISOL) technique, and established within the framework of MYRRHA, the world's first large-scale accelerator driven system project at power levels scalable to industrial systems. The surface ion source, or hot cavity, is chosen as initial source for its reliability and simple design. To account for the higher flux of atoms through this cavity, a theoretical study of the processes within the ion source is discussed here, based on theoretical equations and thermal-electric simulations. In the past, the temperature was clearly identified as a key element to this source, but with the assumption that it remains constant throughout the cavity. Nonetheless, more recent thermal-electric simulations have revealed that the source Ohmic heating leads to temperature gradients along the cavity tube. The temperature profile impact on ionisation in the hot cavity will be reviewed here.

1. Introduction

Given the increased demand for the Radioactive Ion Beams (RIBs) production using the Isotope Separation On-Line (ISOL) technique, a new ISOL facility is currently being built at SCK CEN and is part of the MYRRHA [1] project, the first prototype of a subcritical lead-bismuth cooled reactor driven by a particle accelerator. ISOL@MYRRHA [2] will extract part of the proton beam coming from the accelerator to produce RIBs. By using a high intensity primary beam (100 MeV, up to 0.5 mA proton current) for a longer period of time than existing facilities, the RIB production will be increased while aiming at maintaining the RIB quality. Due to its reliability and simple design, a surface ion source (SIS) or hot cavity was chosen as a first ion source to develop. This ion source is currently used at many other facilities to produce RIBs. Our design [3] stems from the SIS of ISOLDE at CERN [4] and of SPES at INFN [5]. At ISOL@MYRRHA, the higher primary proton beam current will result in a higher atom flux through the ion source. This will likely affect the ion source operation in SIS mode, even more when operating in resonant laser ion source (RILIS) mode [6]. To solve the potential saturation issues and improve the overall production from these ion sources, one needs to understand the key physical mechanisms occurring inside SIS which will help us increase its performance.

2. Surface ionisation principle: from the surface to a tube section

The surface ionisation principle comes from the atoms interaction with a heated surface, leading to the potential gain or loss of a valence electron.

This principle is quantitatively described by two equations [9, 7, 8] with the assumption of an infinite flat surface in contact with vacuum: the ion-to-neutral ratio α_s, and the ionisation efficiency at the surface ε_s, other symbols are identified on table 1:

$$\alpha_s = \frac{n_i}{n_n} = \frac{\sigma_1}{\sigma_0} \exp\left(\frac{\phi - E_i}{k_B T}\right) \quad \text{and} \quad \varepsilon_s = \frac{n_i}{n_i + n_n} = \frac{\alpha_s}{1 + \alpha_s} \tag{1}$$

Those equation parameters depend either on the ionised element (E_i, σ_0, σ_1) or on the hot surface material (ϕ, T). The atom first ionisation energy E_i depicts the minimum energy required to remove the most loosely-bound electron, while the work function ϕ measures how tightly a material holds its electrons, with implications for surface ionisation probability. Noble gases with high ionisation energies E_i are generally difficult to ionise, while elements like potassium and caesium with low ionisation energies are easily ionised. Direct improvement on this parameter E_i is limited, being inherent to the atom's nature.

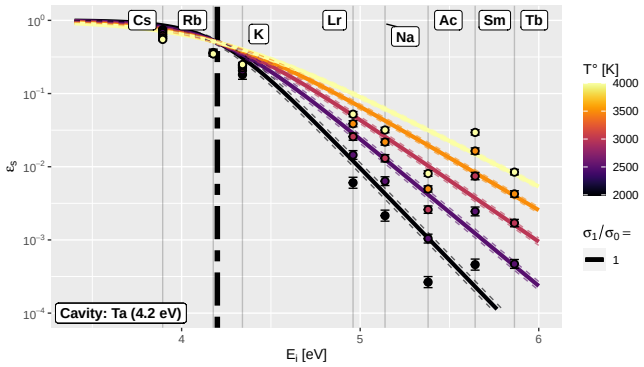

Figure 1: Ionisation efficiency at the surface (eq. 1), as a function of the surface material temperature made of tantalum ($\phi = 4.20 \pm 0.03$ eV). Error bars and dashed lines come from the ϕ uncertainty. The ratio of degeneration of the neutral and ionised electron configuration results in elemental deviations from the lines ($\sigma_1/\sigma_0 = 1$). The dashed vertical line represents $(\phi - E_i) = 0$ for a tantalum surface.

It is the combination of these two parameters $(\phi - E_i)$ which determines the ionisation-efficiency temperature dependence. For cases where $(\phi - E_i) \gg 0$ or ≈ 0, the temperature dependence goes from none to slightly negative. For a tantalum surface ($\phi = 4.2\ eV$), only caesium and rubidium match this case, as seen in figure 1. In the other cases, $(\phi - E_i) \ll 0$, the temperature influence becomes more pronounced as the first ionisation energy E_i of an element increases.

Changing the material work function, so the difference $(\phi - E_i)$, affects the efficiency ε_s for a given element, mainly its temperature dependence. To decrease this ionisation-efficiency temperature dependence, the ϕ can be increased by changing the material surface state or the material itself, from tantalum to tungsten, for example. However, this will likely affect other SIS properties, e.g. mechanical strength or the thermal-electric behaviour.

Like ions, electrons move from the surface to the vacuum through thermal excitation. This thermionic emission described by the Richardson-Dushman equation, was rewritten in the form used in SIS literature [7] in terms of electron number density at the surface wall n_{es} as:

$$n_{es} = Cst \times T^{3/2} \exp\left(-\frac{\phi}{k_B T}\right) \quad \text{with} \quad Cst = 2\left(\frac{2\pi m_e k_B}{h^2}\right)^{3/2} \tag{2}$$

Neutrals, ions and electrons are present in the cavity, resulting in a 'plasma'. Because of the mentioned positive and negative charges, other effects have to be taken into account when considering ionisation inside a hot cavity: charge repulsion, potential field creation, space-charge effect, etc. The formation of a plasma sheath potential [7], induced by the negative and positive charges coming from the surface, is vital for analysing the cavity ionisation efficiency. Two different domains are created: one near the surface, denoted by the subscript s, covered by the previous equations, and one away from the surface, which in the SIS case, is the cavity centre where a plasma forms, denoted by the subscript p.

The Boltzmann relation describes the number density of an isothermal charged particle fluid when the thermal and the electrostatic forces acting on the fluid have reached an equilibrium. If the local electrostatic potential at two nearby locations are Φ_1 and Φ_2, the Boltzmann relation for the electrons takes the form [7]:

$$n_e(\Phi_2) = n_e(\Phi_1)\exp\left(\frac{q_e(\Phi_2-\Phi_1)}{k_B T_p}\right) \quad \Rightarrow \quad \frac{n_{es}}{n_{ep}} = \exp\left(-\frac{q_e\Phi_P}{k_B T}\right) \tag{3}$$

with the surface potential being set to zero ($\Phi_1 = 0$), the difference $\Phi_2 - \Phi_1 = \Phi_P$ is the plasma sheath potential. A plasma in thermal equilibrium at the surface temperature $T_p = T$ is assumed within the cavity, even though this assumption is not necessarily valid [9]. Using the Eggert-Saha equation [7], which states that $\frac{n_{is}n_{es}}{n_{ns}} = C = \frac{n_{ip}n_{ep}}{n_{np}}$, the quasi-neutrality equation $n_{ep} = n_{ip} = n_p$ and a homogeneous neutral density $n_{ns} = n_{np}$, we obtain $n_{ep} = n_{ip} = n_p = \sqrt{n_{es}n_{is}}$. By replacing n_{ep} into the previous equation 3, the Φ_P becomes [7]:

$$\Phi_P = \frac{k_B T}{2q_e}\ln\left(\frac{n_{is}}{n_{es}}\right) = \frac{k_B T}{2q_e}\ln\left(\frac{\alpha_s n_n}{n_{es}}\right) \tag{4}$$

This relation is fundamental to understand the effect of Φ_P on ionisation efficiency and all their related parameters, like the temperature or neutral density. With a $\Phi_P < 0$, whenever an atom is positively surface ionised, it can get trapped inside the potential well formed by the space charges. In this configuration, this confinement potential reinforces surface ionisation. However, if the assumption of thermal equilibrium is not valid in the the overall cavity or even in just a tube section, a factor has to be added to the Eggert-Saha equation, thus affecting the ratio in the Φ_P logarithm part of eq. 4. As such, this factor impact will not hamper the physical reasoning.

This equation can be reversed to get the ratio of ion-to-neutral in the plasma (α_p), which depends on the same ratio at the cavity surface (α_s). The ionisation amplifier role of Φ_P will depend on value and sign of Φ_P [7] by:

$$\alpha_p = \alpha_s\exp\left(-\frac{q_e\Phi_P}{k_B T}\right) = \sqrt{\frac{\alpha_s n_{es}}{n_n}} = \sqrt{\frac{Cst}{n_n}\frac{\sigma_1}{\sigma_0}}\times T^{3/4}\exp\left(-\frac{E_i}{2k_B T}\right) \quad \text{and} \quad \varepsilon_p = \frac{\alpha_p}{1+\alpha_p} \tag{5}$$

One sees that, from the equations above, the surface temperature T and neutral density n_n affect the ionisation efficiency ε_p, but in equilibrium, it becomes independent of the surface material's work function ϕ.

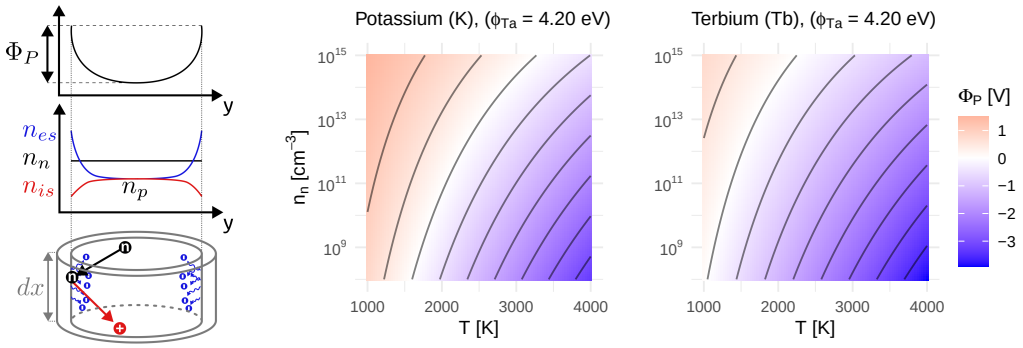

Figure 2: (Left) Schematic representation of the plasma sheath within a tubular hot cavity ($\Phi_P < 0$). (Right) Plasma sheath potential Φ_P on a tantalum surface depending on the surface temperature T and the neutral number density n_n of potassium and terbium. The black lines represent the equipotentials.

Equation 4, represented in figure 2, shows that Φ_P is temperature and element dependent. At a surface temperature equal to 2500 K and a neutral density n_n at $1 \times 10^{10}\ cm^{-3}$, the potential of potassium is at $\Phi_P(K) = -0.72\ V$, and of terbium at $\Phi_P(Tb) = -1.4\ V$. The plasma sheath potential is smaller for easily surface ionisable elements like potassium, which means that at the same temperature on the same surface type, the confinement potential reinforcement will be smaller, but the cavity ionisation efficiency ε_p is still higher because of the higher ionisation efficiency at the surface ε_s. In a realistic case, where a range of elements travels through the cavity, the above equations have to be adapted to integrate the competition between the different elements [7], but this is not discussed here.

3. Electron-bombardment and Ohmic heating

The SIS consists of a high-temperature tube which can be heated using two techniques: electron-bombardment and Ohmic heating, both developed in the early 1970s. **Electron-bombardment heating:** electrons released from hot filaments are accelerated towards a SIS cavity to heat it. These first SIS were developed at Dubna and Livermore using tungsten and tantalum crucibles. The original literature on the SIS [9, 7, 8] was based on results coming from this source type, with a rather homogeneous temperature across the cavity [9]. **Ohmic heating** relies on the Joule effect: a high current passing through the tube, heating the cavity directly due to the material's resistance. The cavity temperature is dependent on the current and the material properties. This applied-current creates also a potential difference along the tubes (ion source and transfer line). If the current's polarity matches the ion-charge type, it will direct ions towards the ion source exit. This Ohmic heating results also in temperature gradients along the tube. For our design this was recently calculated using thermal-electric simulations [3].

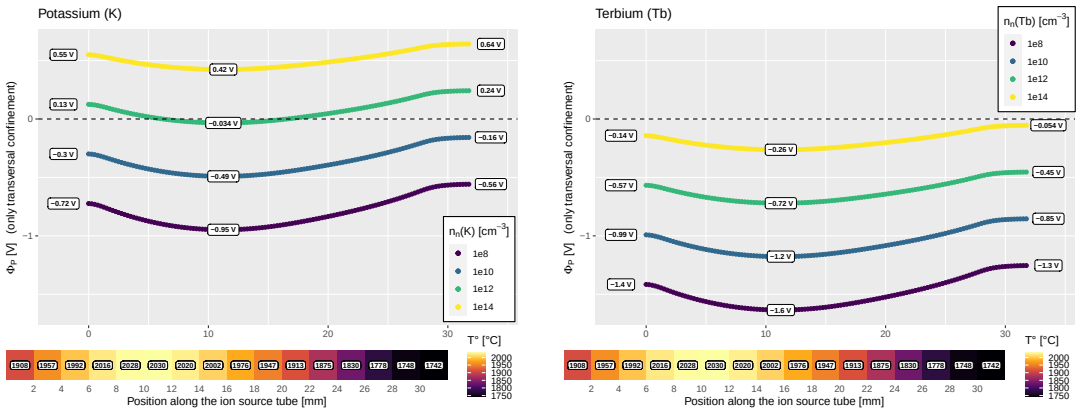

Figure 3: Plasma sheath potential Φ_P on a tantalum surface along the ion source tube depending on its surface temperature. Temperature values come from a thermal-electric simulation with similar boundary conditions as those adopted in reference [3]. The surface potential is set to $\Phi_s = 0$ to better highlight this confinement effect.

With the calculated temperature gradient, the plasma sheath potential Φ_P from equation 4 is shown in figure 3: it varies with the temperature along the ion source tube and increases with increasing neutral density, here taken homogeneous over the cavity. For higher densities, the plasma sheath potential becomes positive at certain colder positions. This means that positive ions in those areas will no longer be properly confined in a negative-charged center, increasing their chance of recombination with the wall and neutralisation. Here, the theoretical equation remains independent of the surface material work function. However, the emergence of a (quasi-) equilibrium, on which these equations rely, is limited by the work function when ions are actively extracted. Again, the validity of the thermal equilibrium assumption remains to be

proven, especially near the cavity end, where the temperature drops and particles are no longer properly confined, but in this work we shall assume it is.

The plasma sheath potential Φ_P (eq. 4) is only a transversal potential difference between the center and the cavity wall ($\Phi_s = 0$). If Φ_P is added on top of the Ohmic potential changes longitudinally along the cavity wall, we obtain figure 4. This Ohmic potential is calculated from thermal-electric simulations. One can see two factors hindering in the ionisation process: the colder spots where surface ionisation is reduced, and zones with a flat or well-shaped potential, especially at lower densities. Ions created here will dwell longer in the cavity, further reducing the capabilities of the cavity plasma to confine new ions. Those two conditions are present at the junction between the ion source and transfer line. The potentials plotted in figures 3 and 4 have been obtained by using an Active Thermal Screen heating system [3], which improves the temperature profile of the ion source, mainly at the exit of the ion source where the extraction electrode is placed, but also at the junction.

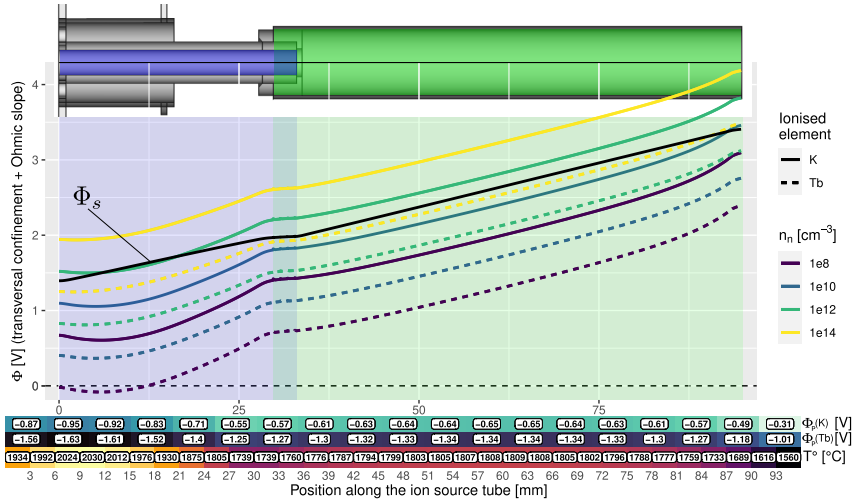

Figure 4: (Top) Schematic cut view of the ion source in blue and transfer line in green. (Bottom) Potential Φ along the ion source tube depending on its surface temperature and potential. Temperature and Ohmic potential Φ_S (black line) values come from a thermal-electric simulation with similar boundary conditions as those adopted in reference [3]. Φ_P calculated on a tantalum surface for K and Tb (plots) with $n_n = 1 \times 10^8\ cm^{-3}$ (values).

4. Conclusion

In this work, the surface ion source theory for a single element has been briefly reconstructed and coupled to the distinct cavity temperature profile of an Ohmically heated tantalum cavity whose design and thermal-electric properties were presented in an earlier work. The combined play of the longitudinal Ohmic potential drop and the transversal plasma sheath potential, which varies with the temperature along the cavity, affects not only the local ionisation efficiency and confinement capability, but also the electric field that drives ions towards extraction. Higher neutral densities, or increased throughput, further suppress the ionisation efficiency and can even lead to a confinement loss at cold spots. Especially the junction between the transfer line and the cavity is sensitive to these effects. Further design optimization both on temperature and on the Ohmic potential drop along the cavity could give way to further efficiency improvement.

Table 1: List of symbols

Subscript s at the surface and p in the plasma.		$\alpha_{s/p}$	Ion-to-neutral ratio. ($\alpha_* = \frac{n_{i*}}{n_{n*}}$)	$\varepsilon_{s/p}$	Ionisation efficiency. ($\varepsilon_* = \frac{\alpha_*}{1+\alpha_*}$)
n_n	Neutral number density.	n_i	Ion number density.	n_e	Electron number density.
$\sigma_{0/1}$	Atomic/Ionic state statistical weight. Data [10].	E_i	First ionisation energy in eV. Data [10].	ϕ	(Surface material) work function in eV. Data [11].
T	(Surface) temperature in K/(°C).	Φ	Potential in V.	Φ_P	Plasma sheath potential in V.

k_B	Boltzmann constant.	h	Planck's constant.	m_e	Electron mass.	q_e	Electron charge.

Acknowledgements This work has been carried out within the scope of a PhD supported by SCK CEN and KULeuven. This research received funding from the MYRRHA project of SCK CEN and Research Foundation Flanders FWO (Belgium) under contract FWO SBO Tb-IRMA-V No. S005019N. It is also part of the PRISMAP project funded within H2020 under grant agreement No. 101008571

References

[1] Aït Abderrahim H, Baeten P, De Bruyn D and Fernandez R 2012 *Energy Conversion and Management* **63** 4–10 10th International Conference on Sustainable Energy Technologies (SET 2011)
[2] Popescu, L 2014 *EPJ Web of Conferences* **66** 10011
[3] Hurier S, Rijpstra K, Creemers P, Ramos J P, Popescu L and Cocolios T E 2022 *J. Phys.: Conf. Ser.* **2244** 012065
[4] Rothe S *et al.* 2023 *Nucl. Instrum. Methods Phys. Res. B* **542** 38–44
[5] Manzolaro M, D'Agostini F, Monetti A and Andrighetto A 2017 *Rev. Sci. Instrum.* **88** 093302
[6] Fedosseev V, Chrysalidis K, Goodacre T D, Marsh B, Rothe S, Seiffert C and Wendt K 2017 *J. Phys. G* **44** 084006
[7] Huyse M 1983 *Nucl. Instrum. Methods Phys. Res.* **215** 1–5
[8] Kirchner R 1990 *Nucl. Instrum. Methods Phys. Res. A* **292** 203–208
[9] Kirchner R 1981 *Nuclear Instruments and Methods in Physics Research* **186** 275–293
[10] NIST Atomic Spectra Database. National Institute of Standards and Technology, Gaithersburg, MD.
[11] Kawano H 2022 *Progress in Surface Science* **97** 100583